



Monitoring quasi-static and cyclic fatigue damage in fibre-reinforced plastics by Poisson's ratio evolution

W. Van Paeppegem *, I. De Baere, E. Lamkanfi, J. Degrieck

Ghent University, Department of Material Science and Engineering, Sint-Pietersnieuwstraat 41, 9000 Gent, Belgium

ARTICLE INFO

Article history:

Available online 20 February 2009

Keywords:

Fatigue
Composites
Fibre-reinforced plastics
Poisson's ratio
Damage

ABSTRACT

Even if the extent of fatigue damage in fibre-reinforced plastics is limited, it can already affect the elastic properties. Therefore, the damage initiation and propagation in composite structures is monitored very carefully. Beside the use of nondestructive testing methods (ultrasonic inspection, optical fibre sensing), the follow-up of the degradation of engineering properties such as the stiffness is a common approach.

In this paper, it is proved that the Poisson's ratio can be used as a sensitive indicator of fatigue damage in fibre-reinforced plastics. Static tests, quasi-static cyclic tests and fatigue tests were performed on $[0^\circ/90^\circ]_{2s}$ glass/epoxy laminates, and longitudinal and transverse strain were measured continuously. The evolution of the Poisson's ratio ν_{xy} versus time and longitudinal strain ϵ_{xx} is studied. As the transverse strain measurement is crucial to monitor the degradation of the Poisson's ratio, three techniques were applied to measure the transverse strain (strain gauges, mechanical extensometer and external optical fibre sensor).

Finally, the technique has been applied to a totally different material: a carbon fabric thermoplastic composite. The results show a very similar degradation of the Poisson's ratio, although no stiffness degradation can be observed during fatigue loading of this material.

It is concluded that the degradation of the Poisson's ratio can be a valuable indicator of fatigue damage, in combination with the stiffness degradation.

© 2009 Elsevier Ltd. All rights reserved.

1. Introduction

Damage in fibre-reinforced composites can take many forms [1,2]: (i) matrix cracks, (ii) fibre–matrix interface failure, (iii) fibre pull-out, (iv) delaminations and (v) fibre fracture. This damage affects the value of the elastic properties at an early stage. Especially in fatigue, the damage initiation phase can cause a pronounced drop of the elastic modulus of 5–10%. In the next damage propagation phase, the stiffness continues to decrease gradually, ranging from a few percent for unidirectionally reinforced carbon composites to several tens of percents for multi-directional glass laminates [3–7].

Most one-dimensional damage models for fibre-reinforced composites only account for the effect of damage on the stiffness [8–16]. The degradation of the Poisson's ratio is not included in these models. Nevertheless this degradation has been observed and is not negligible [17–20]. Bando et al. showed that the Poisson's ratio of a carbon/epoxy UD laminate can drop by 50% under static tensile loading [19], while Pidaparti and Vogt proved that the Poisson's ratio is a very sensitive parameter while monitoring fatigue damage in human bone [20].

In this paper, it is proved that the Poisson's ratio can be used as a sensitive indicator of damage in fibre-reinforced composites for both static, cyclic and fatigue loading. Just like the stiffness, it can be measured accurately and nondestructively. Further, it gives information about the damage state of the off-axis plies in a multi-directional composite laminate.

In a first step, static tensile tests are performed on $[0^\circ/90^\circ]_{2s}$ glass/epoxy laminates, followed by quasi-static cyclic loading–unloading tests. As the observed behaviour of the Poisson's ratio is quite peculiar, the measurement method of the transverse strain can be questioned. Therefore the transverse strain has been measured by three methods: transverse strain gauge, mechanical extensometer and external optical fibre sensor.

Next the strain-controlled fatigue tests on the $[0^\circ/90^\circ]_{2s}$ glass/epoxy laminates are discussed. They show excellent agreement with the observed behaviour in quasi-static cyclic tests. Final validation is done by applying the measurement technique to a totally different composite: a carbon fabric/PPS thermoplastic composite.

2. Material and test methods

The material under study was a glass/epoxy composite. The glass reinforcement was a unidirectional E-glass fabric (Roviglas

* Corresponding author. Fax: +32 0 9 264 35 87.

E-mail address: Wim.VanPaeppegem@UGent.be (W. Van Paeppegem).

R17/475). In the fibre direction \vec{e}_{11} , the reinforcement was 475 g/m², while in the direction \vec{e}_{22} , the reinforcement was 17 g/m². The epoxy matrix was Araldite LY 556.

Three stacking sequences were manufactured: $[0^\circ]_8$, $[90^\circ]_8$ and $[0^\circ/90^\circ]_{2s}$ with the angle referred to the direction \vec{e}_{11} . The layups $[0^\circ]_8$ and $[90^\circ]_8$ were used for characterization in the orthotropic material directions, while $[0^\circ/90^\circ]_{2s}$ was used for the study of the Poisson's ratio.

All specimens were manufactured by vacuum assisted resin transfer moulding with a closed steel mould. The nominal thickness of all specimens was 3.0 mm and the fibre volume fraction was between 48% and 50%. The specimens were cut to dimensions on a water-cooled diamond tipped saw.

The inplane elastic properties of the individual $[0^\circ]$ glass/epoxy lamina were determined by the dynamic modulus identification method described by Sol et al. [27,28] and are listed in Table 1. The modulus E_{11} corresponds to the fibre direction \vec{e}_{11} , while the modulus E_{22} corresponds to the direction \vec{e}_{22} . The Poisson's ratio ν_{12} and shear modulus G_{12} are listed as well. Due to the strongly anisotropic nature of the unidirectional fabric, there is a large difference between both moduli.

Apart from the dynamic modulus identification method, static tensile tests on the $[0^\circ]_8$ and $[90^\circ]_8$ layups were performed to check the values of the elastic properties and to determine the static strengths.

The values of X_T and ϵ_{11}^{ult} were derived from the $[0^\circ]_8$ tests, while Y_T and ϵ_{22}^{ult} were derived from the $[90^\circ]_8$ tensile tests. The average values are listed in Table 2.

It is important to mention that the mechanical behaviour in the \vec{e}_{11} and \vec{e}_{22} direction is quasi-linear until failure, as shown in Fig. 1 and Fig. 2.

In this manuscript, only the $[0^\circ/90^\circ]_{2s}$ sequence has been considered for studying the evolution of the Poisson's ratio, because a lot of researchers have proved that in case of transverse matrix cracking in the 90° plies, the Poisson's ratio ν_{xy} should decrease [21–26].

3. Static measurements of ν_{xy}

The elastic and strength properties of the $[0^\circ/90^\circ]_{2s}$ laminate were determined by quasi-static tensile tests on an Instron electro-mechanical testing machine. The tensile tests were displacement-controlled with a displacement speed of 1 mm/min.

The specimen geometry is illustrated in Fig. 3. The nominal specimen width was 34 mm and the thickness 3 mm. The gauge length was 140 mm. The tests were done in accordance with ASTM D3039 "Standard Test Method for Tensile Properties of Polymer Matrix Composite Materials". Two strain gauges were applied in the X- and Y-direction. The used strain gauges are "general purpose Strain Gauges" from VISHAY micro-measurements. The grid resistance is $350.0 \pm 0.3\% \Omega$ and they have a gauge factor of 2.105. The strain gauges are bonded using the M-BOND 200 adhesive from Vishay micro-measurements. For the actual measurement, a stabilised 350 Ω Wheatstone bridge, type SGA 503 from CIL is used; each strain gauge has its own amplifier to which the gauge is attached using a three-wire connection. A shunt calibration is performed for every single experiment.

Table 1
Inplane elastic properties of the individual $[0^\circ]$ glass/epoxy lamina.

E_{11} [GPa]	38.9
E_{22} [GPa]	13.3
ν_{12} [-]	0.258
G_{12} [GPa]	5.13

Table 2
Tensile strength properties of the individual glass/epoxy lamina.

X_T [MPa]	901.0
ϵ_{11}^{ult} [-]	0.025
Y_T [MPa]	36.5
ϵ_{22}^{ult} [-]	0.0025

The noise on the strain gauge measurement is about 15 micro-strain. As the measured transverse strains are in the order of 1000 microstrain, the error is about 0.15% on the maximum strain signal.

The major Poisson's ratio ν_{xy} is defined as $-\epsilon_{yy}/\epsilon_{xx}$ (in the x - y coordinate system of Fig. 3). If the term Poisson's ratio is used, we always refer to the major Poisson's ratio ν_{xy} .

Fig. 4 shows the stress-strain curve for the $[0^\circ/90^\circ]_{2s}$ specimens IF4 and IF6. In the first measurement, the strain gauge signal was lost at about 1.0% longitudinal strain (due to debonding), but the load signal was measured until failure. The calculated failure stresses were 465.5 MPa and 447.7 MPa, respectively. The failure strain of specimen IF6 was 0.0208 (or 2.08%).

The value of the elastic modulus E_{xx} was 27.56 GPa and 30.92 GPa, respectively, (determined by least-squares linear fit for the strain range $[0;0.0025]$). The value measured by the dynamic modulus identification method was 31.10 GPa for another specimen from the same batch of material.

At a level of about 100 MPa longitudinal stress, there is a small change in the slope of the stress-strain curve. The corresponding strain is slightly higher than 0.0025 (0.25%) which is the fracture strain of the 90° plies in the cross-ply laminate (see Table 2).

The corresponding history of the Poisson's ratio ν_{xy} versus ϵ_{xx} is shown in Fig. 5. Although the longitudinal stress-strain curve is almost linear (Fig. 4), the Poisson's ratio is decreasing quite fast. This is due to early transverse matrix cracking of the 90° plies. Indeed the failure strain ϵ_{22}^{ult} of the 90° plies equals only 0.0025 (see Table 2) and once the longitudinal strain in these plies exceeds this threshold, the 90° plies are severely cracked. The estimated value of ν_{xy} in the elastic regime is 0.141 and 0.152 for IF4 and IF6, respectively. The calculated value of ν_{xy} from the dynamic modulus identification method is 0.162.

There is no explanation for the different initial behaviour of the two curves, except the observation that the calculation of ν_{xy} for very small longitudinal strain (and thus even smaller transverse strain) can yield quite different values from specimen to specimen. Also some initial relaxation of the strain gauge adhesive might be present.

4. Measurements of ν_{xy} under quasi-static cyclic loading

In order to observe the behaviour of the Poisson's ratio under repeated loading, quasi-static cyclic tensile tests are performed. The displacement speed was 2 mm/min and the load cycles between 1 kN and subsequent load levels of 20, 20, 25, 35, 35, 42, 45, 48 and 54.7 kN (failure load), as shown in Fig. 6. The small change of the slope in the curve at 10 kN corresponds with a longitudinal stress σ_{xx} of 102.4 MPa. This knee-point could indeed be observed in the stress-strain curves in Fig. 4.

The corresponding time history of the measured longitudinal strain ϵ_{xx} and the transverse strain ϵ_{yy} for the cyclic tensile test on the $[0^\circ/90^\circ]_{2s}$ specimen IF3 is shown in Fig. 7. At the lowest loads of 1 kN, the transverse strain ϵ_{yy} becomes slightly positive. This is not caused by improper calibration of the strain gauges. The strain measurement channels are calibrated for each strain gauge with a precision shunt resistance. It will be shown in subsequent figures that this effect is very reproducible.

Both the failure stress and failure strain are higher than in the quasi-static tensile tests. The failure stress here is 560 MPa and

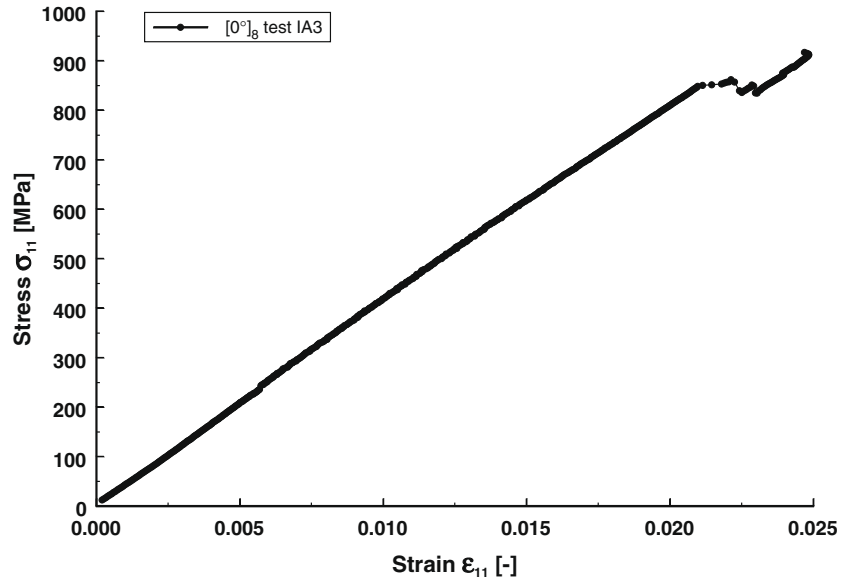


Fig. 1. Stress–strain curve for static $[0^\circ]_8$ tensile test IA3.

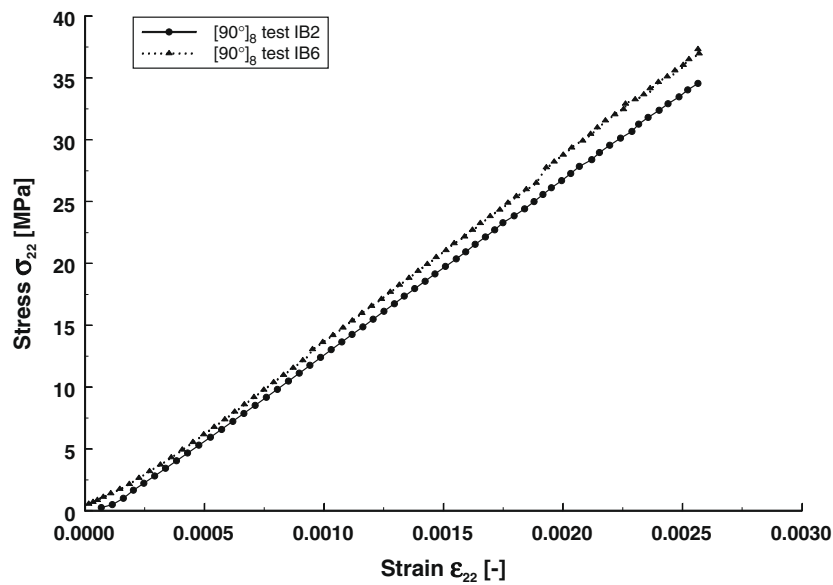


Fig. 2. Stress–strain curve for static $[90^\circ]_8$ tensile tests IB2 and IB6.

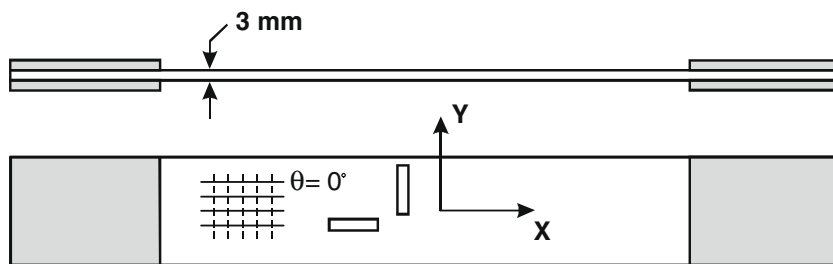


Fig. 3. Layout of $[0^\circ/90^\circ]_{2s}$ glass/epoxy specimens.

the failure strain 0.0293 (or 2.93%). This strengthening effect might be due to a better fibre alignment. A similar phenomenon was already reported by the authors for cyclic loading–unloading tests of $[+45/-45]_{2s}$ glass/epoxy laminates [29,30].

In Fig. 8, the evolution of the Poisson's ratio ν_{xy} is plotted against the longitudinal strain ϵ_{xx} , together with its evolution in the quasi-static tensile tests IF4 and IF6 (see Fig. 5). It can be clearly seen that the maxima of the cyclic ν_{xy} curves follow the static curve very well

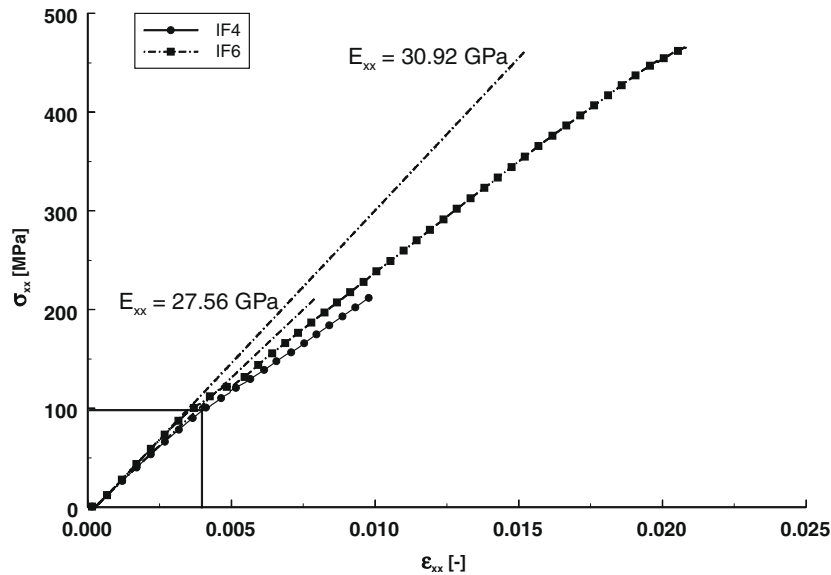


Fig. 4. Stress–strain curve for the static tensile test of the $[0^\circ/90^\circ]_{2s}$ specimens IF4 and IF6.

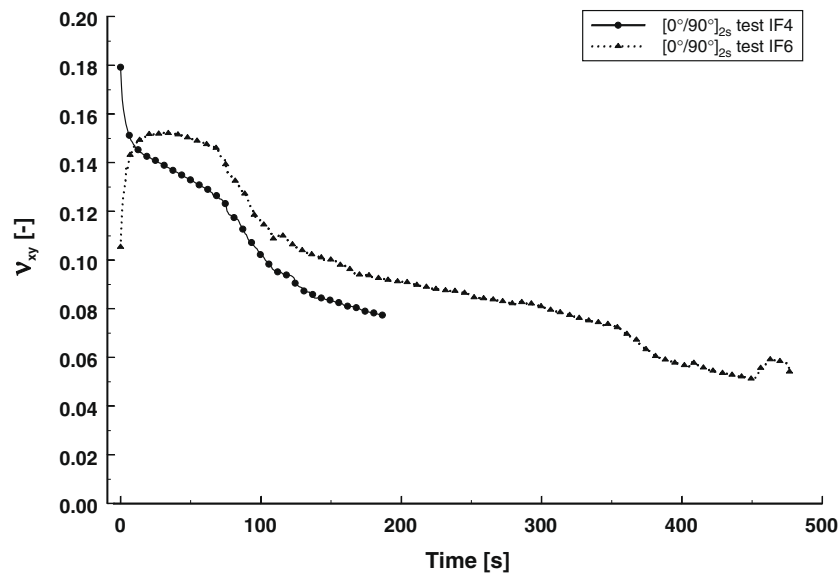


Fig. 5. Evolution of the Poisson's ratio ν_{xy} depending on the longitudinal strain ε_{xx} for the $[0^\circ/90^\circ]_{2s}$ specimens IF4 and IF6.

for the ε_{xx} range $[0; 0.015]$. As the Poisson's ratio changes drastically during unloading, its value must be stress dependent because no further damage occurs during unloading.

Fig. 9 shows the corresponding time history of the Poisson's ratio ν_{xy} . In the region of low forces (and thus low strains ε_{xx}), the Poisson's ratio ν_{xy} becomes negative, due to the slightly positive value of the transverse strain ε_{yy} for small loading values (see Fig. 7).

Although this peculiar behaviour of the Poisson's ratio has been observed for several other specimens, it can be questioned whether this is an intrinsic material behaviour or an artefact of the measurement method, for example due to the effect of the multiple transverse cracks in the 90° plies on the bonding quality of the transverse strain gauge.

Therefore other measurement methods have been considered. The first one was the use of a transverse extensometer. This transverse extensometer was mounted on the specimen, together with a longitudinal and transverse strain gauge, as shown in Fig. 10.

The longitudinal stress–strain curves imposed on the $[0^\circ/90^\circ]_{2s}$ specimen IE3 are shown in Fig. 11. The first four cycles were limited to a longitudinal stress of 100 MPa, the threshold value in Fig. 4. Next, the load was increased with 50 MPa every cycle. The displacement speed was 2 mm/min.

The corresponding transverse strain measurements with both the transverse strain gauge (black line) and the transverse extensometer (black line with open circles) are shown in Fig. 12. The sample numbers are directly proportional with time, since both signals were sampled with the same constant sample rate. The correspondence between the strain signals is good and also the transverse extensometer measurement shows a slightly positive transverse strain after a few cyclic loading cycles. The small difference in peak values and gradient can be due to small settlements of the extensometer blades.

The calculated time history of the Poisson's ratio ν_{xy} from both transverse strain signals is shown in Fig. 13. For both time histories, the same longitudinal strain measurement is used for the calculation of the Poisson's ratio.

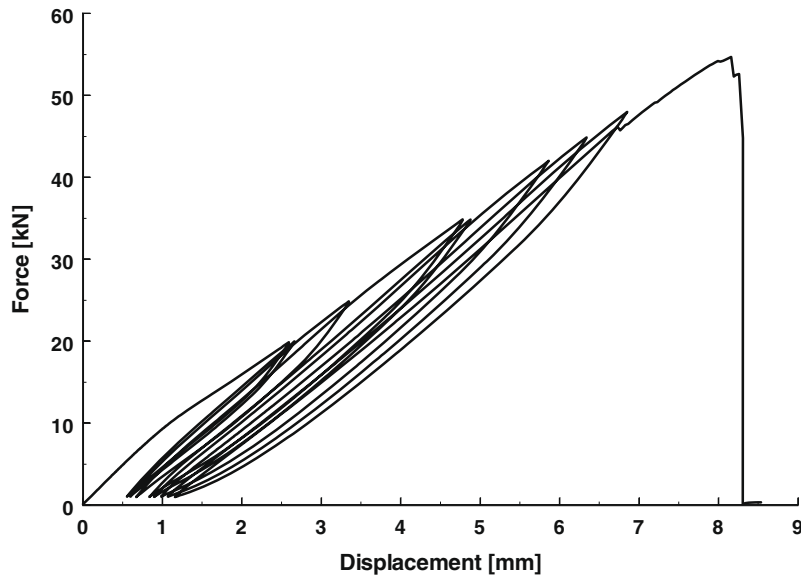


Fig. 6. Quasi-static cyclic tensile force–longitudinal displacement curve of $[0^\circ/90^\circ]_{2s}$ specimen IF3.

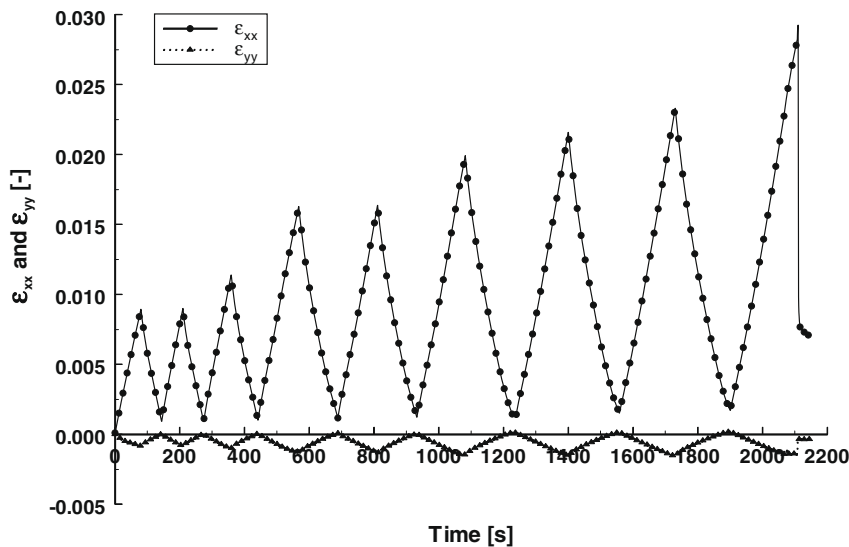


Fig. 7. Time history of ε_{xx} and ε_{yy} for the quasi-static cyclic test of $[0^\circ/90^\circ]_{2s}$ specimen IF3.

The corresponding history of the Poisson's ratio versus longitudinal strain is shown in Fig. 14. Again the typical nonlinear behaviour of the Poisson's ratio is present.

A third method of transverse strain measurement was the use of an external optical fibre sensor. For measuring strain, broadband light is transmitted into the optical fibre. At a specific point in this fibre, there is a Bragg grating, which acts as a wavelength selective mirror. The so-called Bragg wavelength, λ_B is reflected with a Full Width at Half Maximum of typically 100 pm, while all other wavelengths are transmitted. A fibre Bragg grating is actually no more than an area in the core of the fibre with successive zones with an alternating refractive index. The period of this grating is directly proportional with the reflected Bragg wavelength. If strain is imposed on the grating, the period of the grating changes and thus also the value of the reflected Bragg wavelength. As such, a measurement of the strain is achieved: the difference between the wavelength of the strained and the unstrained grating increases linearly with the imposed strain. The sensitivity is 1.2 picometer per microstrain at the operating wavelength of 1.5 μm .

This is an absolute value, since it only depends on the geometry of the grating and the elasto-optic constants of the glass, and not on any form of electronic manipulation such as filtering or amplifying. Furthermore, it has to be noticed that a fibre Bragg grating written in hydrogenated fibres will notice a decrease of refractive index modulation of approx. 15% hence a drift of Bragg wavelength and decrease of reflection of about 9% in the first few weeks after fabrication of the grating. However this is not the case for gratings written in non-hydrogenated fibres, as is the case for the fibre Bragg gratings employed in these experiments. As such, the Bragg wavelength of these sensors does not drift away in time. The used data acquisition system has an accuracy of 5 pm and it is constant in time. Therefore, this system also does not cause a drift of the measurement.

Fig. 15 shows the externally bonded optical fibre sensor before (left) and after (right) quasi-static cyclic testing of the glass/epoxy laminate. The fibre optic sensors used for these embedding experiments are Draw Tower fibre Bragg gratings (DTG®'s), provided by FBGS-Technologies GmbH, Jena (Germany). Such gratings are

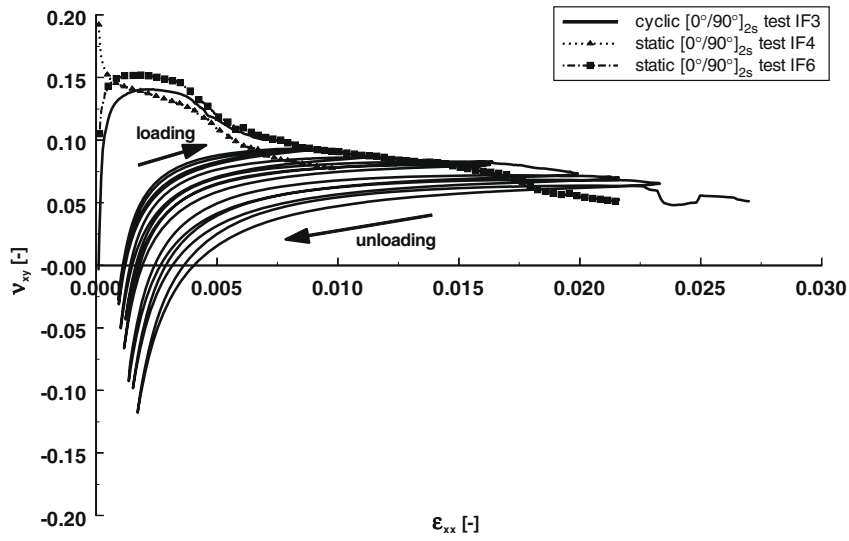


Fig. 8. Evolution of the Poisson's ratio ν_{xy} depending on the longitudinal strain ϵ_{xx} for the quasi-static cyclic test of $[0^\circ/90^\circ]_{2s}$ specimen IF3.

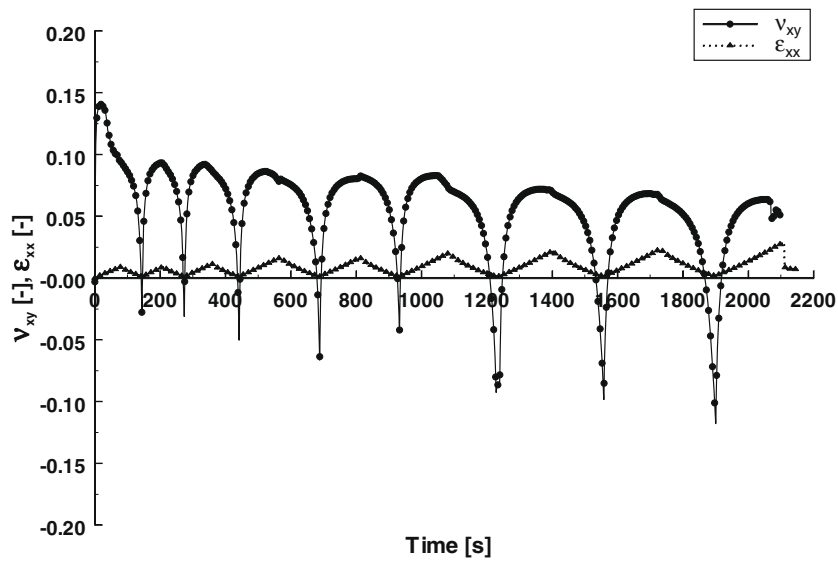


Fig. 9. Time history of the Poisson's ratio ν_{xy} for the quasi-static cyclic test of $[0^\circ/90^\circ]_{2s}$ specimen IF3.

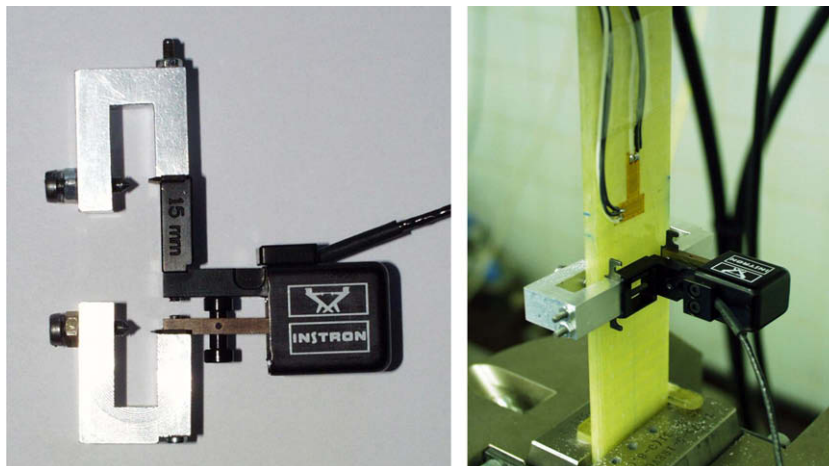


Fig. 10. Design and mounting of transverse extensometer.

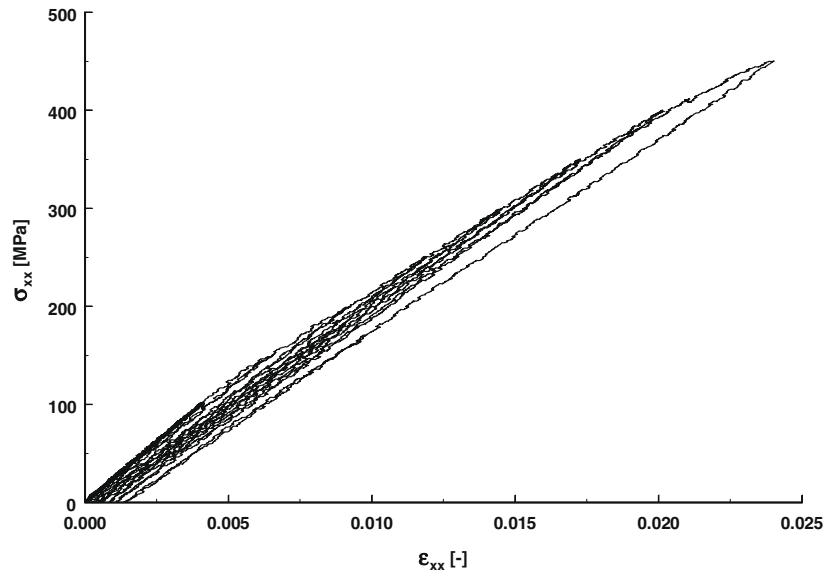


Fig. 11. Quasi-static cyclic stress–strain curves for $[0^\circ/90^\circ]_{2s}$ specimen IE3.

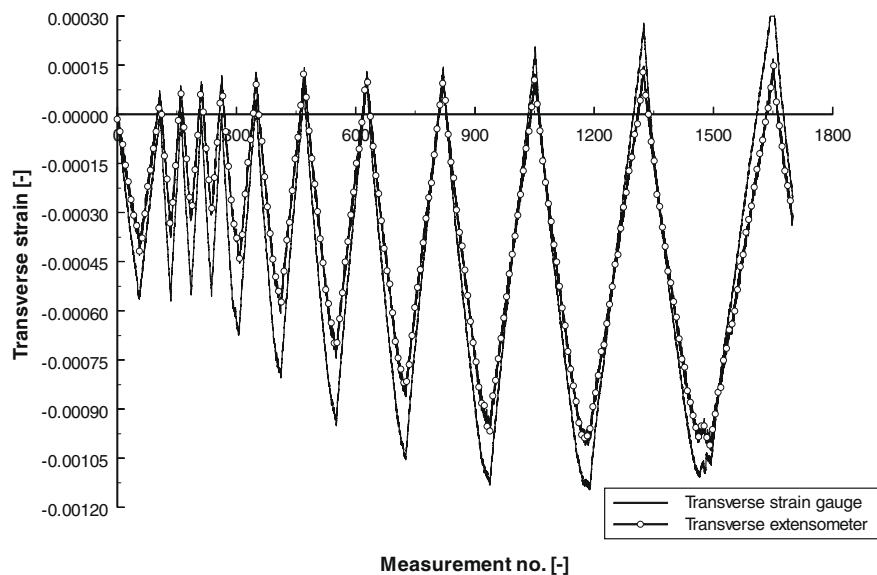


Fig. 12. Transverse strain measurement by transverse strain gauge and transverse extensometer for quasi-static cyclic test on $[0^\circ/90^\circ]_{2s}$ specimen IE3.

manufactured during the fabrication process of the optical fibre and are coated just after the inscription of the Bragg grating. The FBG's are written in a Single Mode optical fibre with core diameter of $6\ \mu\text{m}$ and cladding diameter of $125\ \mu\text{m}$ and they have a typical length of about 8 mm. First, the surface of the specimen was degreased with acetone and then the fibre was bonded over the entire width of the specimen, using a two-component epoxy adhesive, designed for bonding strain gauges.

The quasi-static cyclic test was done as follows: first four cycles were done till a maximum stress level of 50 MPa at 2 mm/min. Next the maximum load of each loading step was increased with 50 MPa until 350 MPa was reached. Fig. 16 shows the comparison between the signals of the transverse strain gauge (black line) and the external optical fibre sensor (black line with open circles) from 50 MPa till 350 MPa loading. The optical data were registered with a FBG-scan interrogator. The quantitative values do not correspond very well, but the same trend can be observed. The main reason for the difference in measured values is the inaccurate strain transfer

from the laminate to the external optical fibre, due to the large amount of adhesive that is spread over the optical fibre sensor. It will be shown later that the observations are confirmed, if an external optical fibre sensor with a very thin bonding line of adhesive is used.

Combining the observations from the three different measurement methods, it can be concluded that the measurements of the bonded transverse strain gauge can be considered reliable, and as a consequence, also the derived values of the Poisson's ratio.

5. Measurements of ν_{xy} under cyclic fatigue loading

In order to assess the sensitivity of the Poisson's ratio ν_{xy} under fatigue loading, tension–tension fatigue tests with a sinusoidal wave form have been conducted on the same material. All tests were carried out at room temperature and ambient humidity. The specimen geometry was the same as shown in Fig. 3, but the longitudinal strain gauge was replaced by an extensometer. The

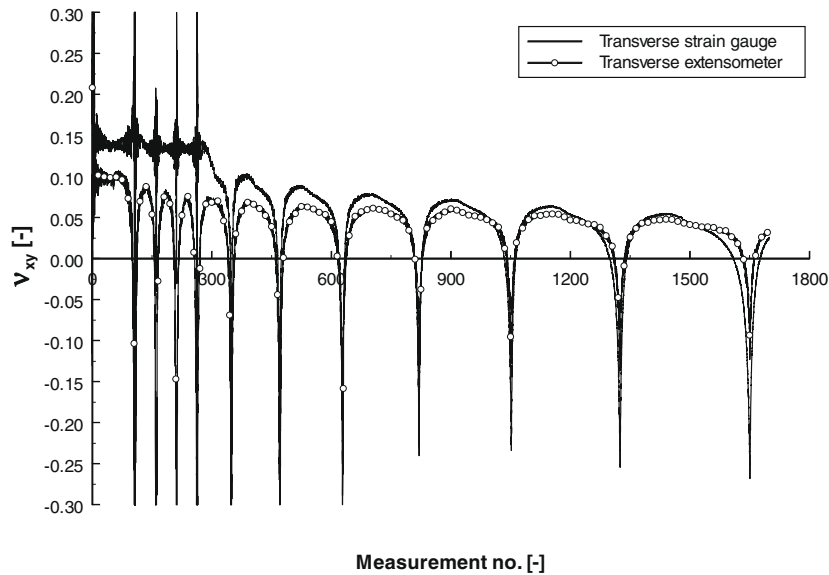


Fig. 13. Time history of the Poisson's ratio from both transverse strain signals for quasi-static cyclic test on $[0^\circ/90^\circ]_{2s}$ specimen IE3.

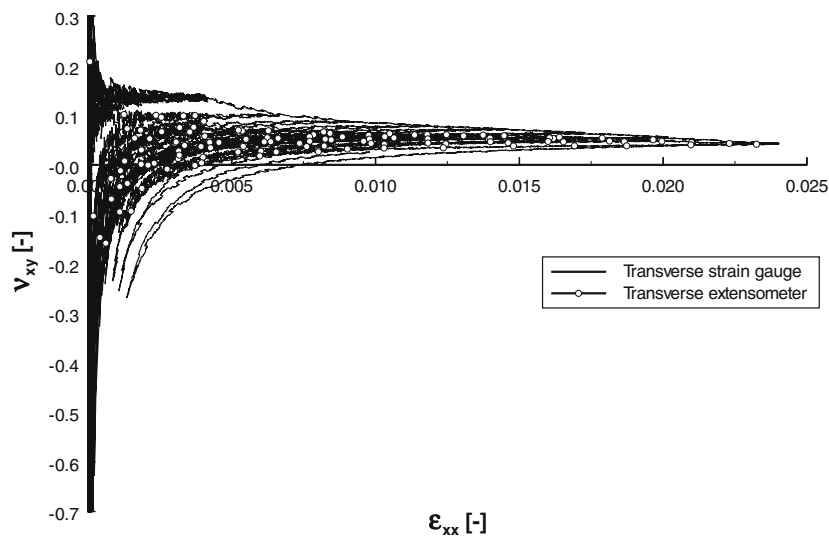


Fig. 14. Evolution of the Poisson's ratio v_{xy} depending on the longitudinal strain ϵ_{xx} for the quasi-static cyclic test of $[0^\circ/90^\circ]_{2s}$ specimen IE3.

fatigue tests were strain-controlled, so that the measurement of the transverse strain ϵ_{yy} immediately yields the value of the Poisson's ratio v_{xy} .

The maximum strain level was chosen 0.006 (0.6%), because this strain level is slightly higher than the knee-point in the static stress–strain curve (see Fig. 4). Using a “strain ratio” R of 0.1 (similar to the stress ratio in fatigue), the minimum strain level is 0.0006 (0.06%).

The fatigue tests were done at 2 Hz on an Instron servohydraulic testing machine.

Fig. 17 shows the clamped specimen with its instrumentation. The extensometer measures the longitudinal strain, the transverse strain gauge measures the transverse strain and a thermocouple monitors the surface temperature of the composite laminate. Load and displacement were measured by the servohydraulic machine control. The strain-control is done by the extensometer.

Normally, the life time of strain gauges in fatigue is very limited, because the maximum strain levels they can endure in fatigue, are very much reduced compared to static operation. However, in this

case the transverse strain levels were very small (a few hundred microstrains) and no temperature rise of the surface was detected from the thermocouple.

The signals of load, displacement, extensometer, strain gauge and temperature were each sampled at 100 Hz every 5 min for five subsequent loading cycles using a National Instruments NI DAQ-PAD-6052E measurement card and LabVIEW software.

For the first cyclic fatigue test W_090_7, 7500 loading cycles were applied. The stress–strain curve was measured before fatigue testing, but only to a very low longitudinal strain of 0.001 (0.1%), because the failure strain of the 90° plies is only 0.0025 (0.25%) (see Table 2). After stopping the fatigue test, the same static tensile test was repeated. A small degradation of the longitudinal stiffness E_{xx} was observed from 29.77 GPa to 27.37 GPa.

In Fig. 18, the evolution of the Poisson's ratio v_{xy} is again plotted against the longitudinal strain ϵ_{xx} for different sets of five measured cycles. The shape of the loading–unloading curves is very similar to the one showed in Fig. 8. It must be noticed as well that the Poisson's ratio shows a sharp decline during the first loading

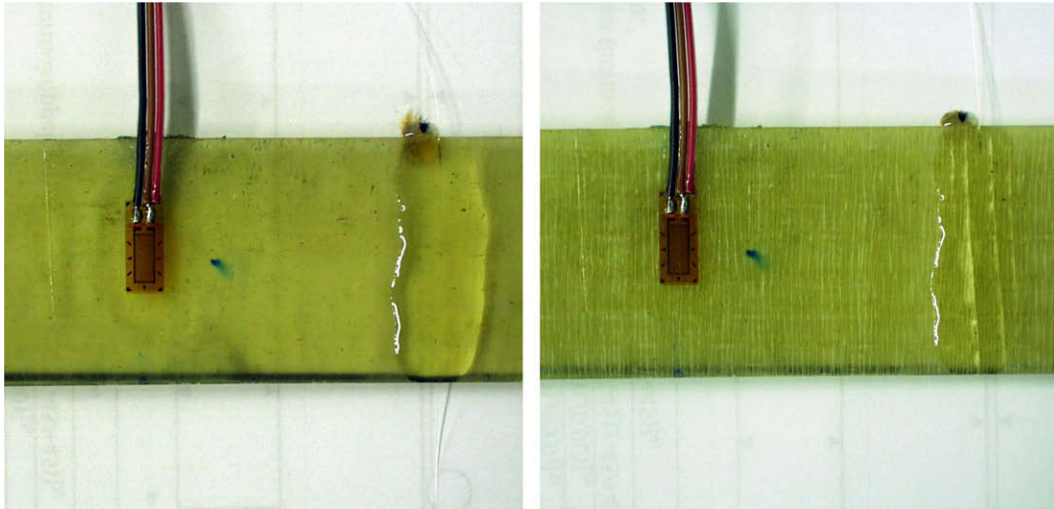


Fig. 15. Externally bonded optical fibre sensor before (left) and after (right) cyclic testing.

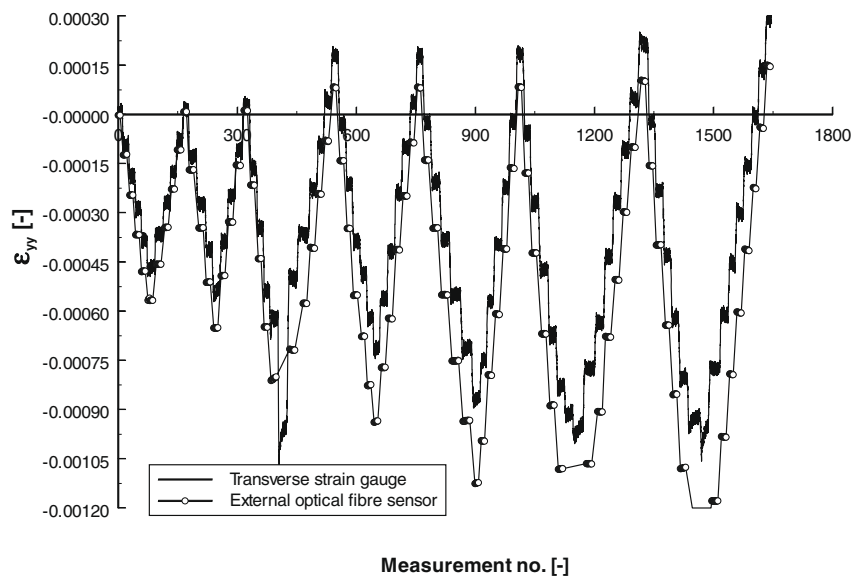


Fig. 16. Transverse strain measurement by transverse strain gauge and external optical fibre sensor for quasi-static cyclic test on $[0^\circ/90^\circ]_{2s}$ specimen IE6.

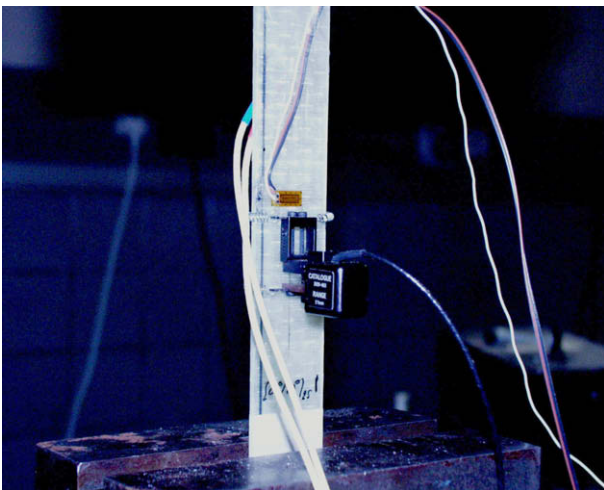


Fig. 17. Instrumentation of the $[0^\circ/90^\circ]_{2s}$ glass/epoxy specimens.

cycles. After only 600 cycles, the value has already decreased considerably.

Next, another specimen W_090_8 was tested for a larger number of cycles. In Fig. 19, the evolution of the Poisson's ratio ν_{xy} is plotted against the longitudinal strain ϵ_{xx} for three sets of five measured cycles. The correspondence with Fig. 8 is again very good.

Fig. 20 shows a magnified view of the $\nu_{xy}-\epsilon_{xx}$ curves. It seems that both the maximum and minimum value of the Poisson's ratio are affected by the fatigue damage and could be a usable damage variable.

To be sure that the shape of the $\nu_{xy}-\epsilon_{xx}$ curves is not due to strain rate effects, the evolution of the Poisson's ratio ν_{xy} versus longitudinal strain ϵ_{xx} was measured under static loading conditions as well, to eliminate strain rate effects. The static test before fatigue testing was again done to a very low longitudinal strain of 0.001 (0.1%), because the failure strain of the 90° plies is only 0.0025 (0.25%) (see Table 2). The intermediate static tests at $N=7\,500$ cycles and $N=22\,800$ cycles were done in the same strain range of 0.0006 (0.06%)–0.006 (0.6%) as the fatigue cycling.

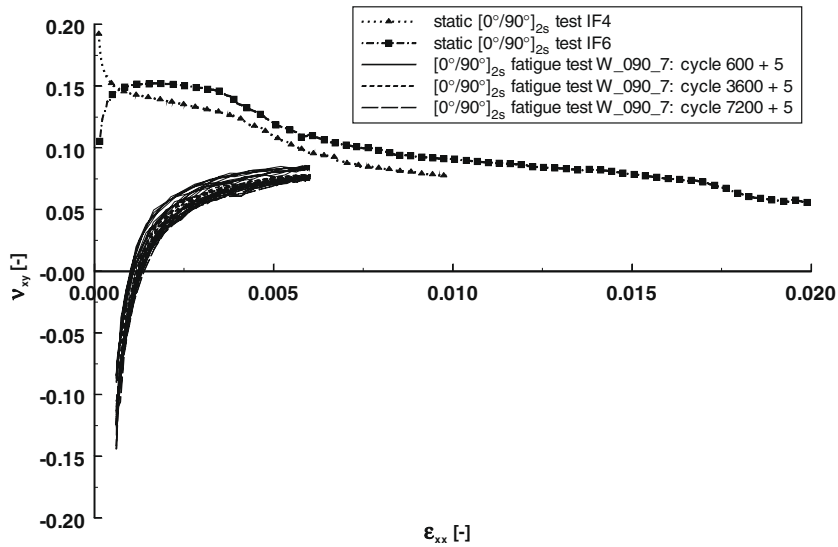


Fig. 18. Evolution of the Poisson's ratio ν_{xy} depending on the longitudinal strain ϵ_{xx} for the $[0^\circ/90^\circ]_{2s}$ specimen W_090_7 at three chosen intervals in the fatigue test.

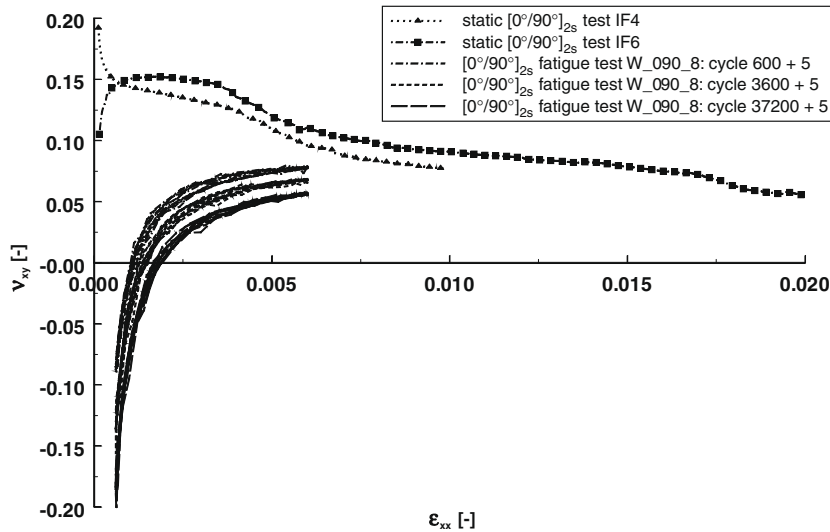


Fig. 19. Evolution of the Poisson's ratio ν_{xy} depending on the longitudinal strain ϵ_{xx} for the $[0^\circ/90^\circ]_{2s}$ specimen W_090_8 at three chosen intervals in the fatigue test.

Fig. 21 shows that the initial Poisson's ratio ν_{xy} is about 0.15 [-]. The scatter is quite large in the initial strain regime, due to the very low longitudinal strains ϵ_{xx} and even lower transverse strains ϵ_{yy} . However, for longitudinal strains ϵ_{xx} larger than approximately 0.0005, the Poisson's ratio converges to a more or less constant value of 0.15. In the intermediate static tests at cycles 7500 and 22,800, the same shape of the $\nu_{xy}-\epsilon_{xx}$ curve appears as shown in Fig. 19. That means that the shape of the $\nu_{xy}-\epsilon_{xx}$ curves is not affected by the real-time measurement during the fatigue loading.

Finally, to see if the observed behaviour of the Poisson's ratio ν_{xy} is dependent on the type of material, all tests have been repeated on a thermoplastic composite with a 5-harness satin weave carbon fibre fabric and polyphenylene sulphide (PPS) matrix. The stacking sequence was $[(0^\circ,90^\circ)]_{4s}$ where $(0^\circ,90^\circ)$ represents one layer of fabric.

This material shows no observable stiffness degradation in cyclic fatigue. Furthermore, the Poisson's ratio of about 0.05 is very small [31]. Cyclic fatigue tests on this material were performed in load-control with a maximum applied stress of 550 MPa (stress ratio $R = 0.0$) and test frequency of 2 Hz. Load-control was chosen

over strain-control to see if this parameter had any influence on the evolution of the Poisson's ratio. The specimens were 30 mm wide and had a gauge length of 150 mm. All tests were performed at ambient temperature and humidity.

Fig. 22 shows the evolution of the Poisson's ratio ν_{xy} depending on the longitudinal strain ϵ_{xx} for the $[(0^\circ,90^\circ)]_{4s}$ carbon/PPS specimen K6 at the running-in of the fatigue test. During running-in, the amplitude of the load-controlled fatigue cycles gradually builds up within the pre-set envelope time. During these first loading cycles, a gradual change of the value of the Poisson's ratio can be observed, starting from a steady value of about 0.05 towards more and more negative values. By the time that the evolution is shown at $N = 50$ cycles (see Fig. 23), the Poisson's ratio remains always negative.

Fig. 23 shows the evolution of the Poisson's ratio ν_{xy} depending on the longitudinal strain ϵ_{xx} for the same $[(0^\circ,90^\circ)]_{4s}$ carbon/PPS specimen K6 at six chosen intervals in the load-controlled fatigue test. Again the typical shape of the $\nu_{xy}-\epsilon_{xx}$ curves is observed and they clearly shift to lower values with increasing number of loading cycles.

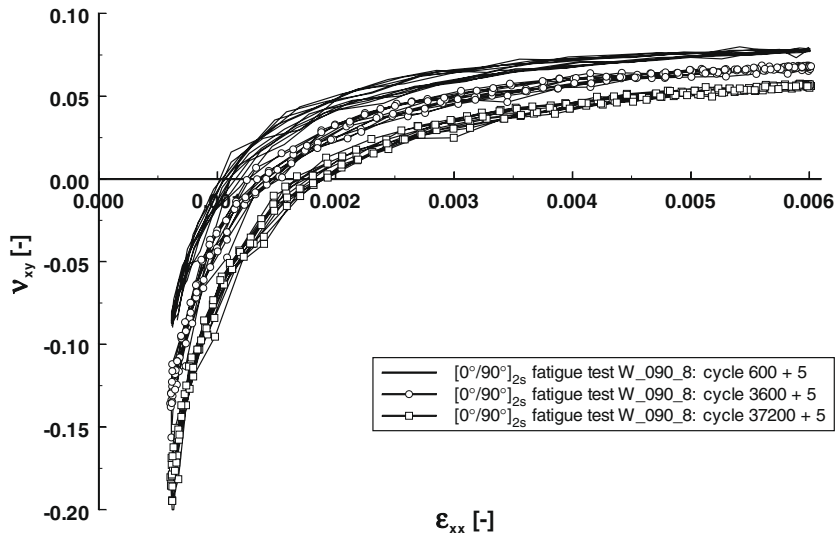


Fig. 20. Evolution of the Poisson's ratio v_{xy} depending on the longitudinal strain ϵ_{xx} for the $[0^\circ/90^\circ]_{2s}$ specimen W_090_8 at three chosen intervals in the fatigue test (magnified view).

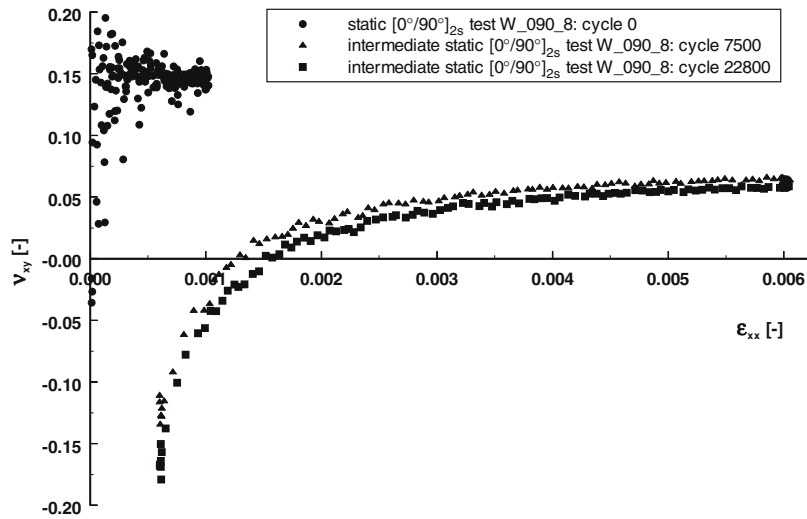


Fig. 21. Evolution of the Poisson's ratio v_{xy} depending on the longitudinal strain ϵ_{xx} for the initial and intermediate static tensile tests of the $[0^\circ/90^\circ]_{2s}$ fatigue test W_090_8.

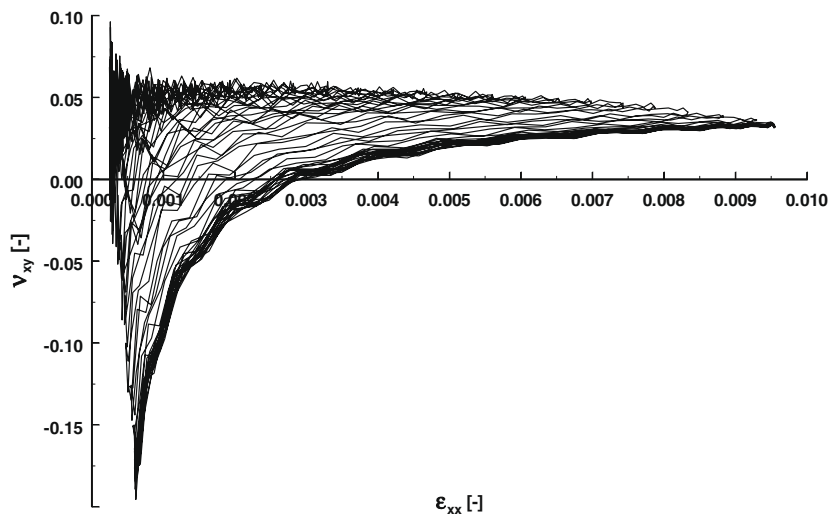


Fig. 22. Evolution of the Poisson's ratio v_{xy} depending on the longitudinal strain ϵ_{xx} for the $[(0^\circ/90^\circ)]_{4s}$ carbon/PPS specimen K6 during running-in of the fatigue test.

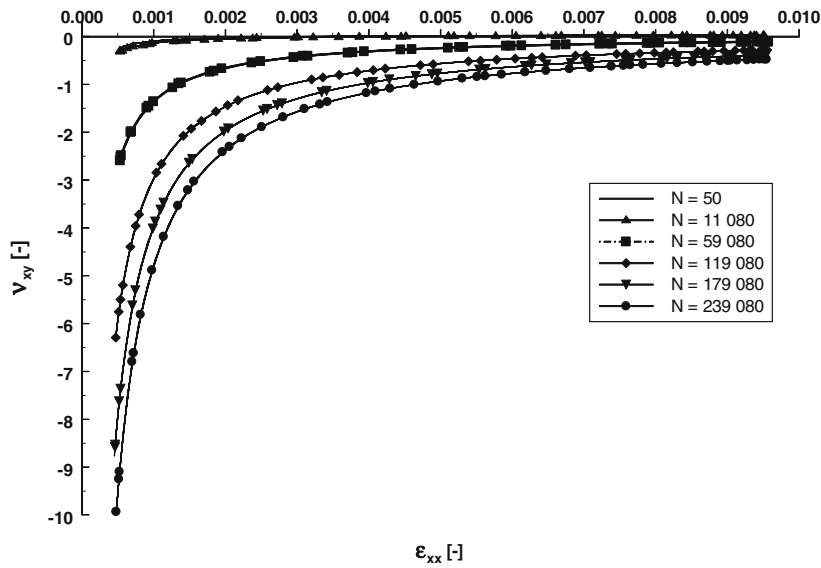


Fig. 23. Evolution of the Poisson's ratio ν_{xy} depending on the longitudinal strain ϵ_{xx} for the $[(0^\circ/90^\circ)]_{4s}$ carbon/PPS specimen K6 at six chosen intervals in the fatigue test.

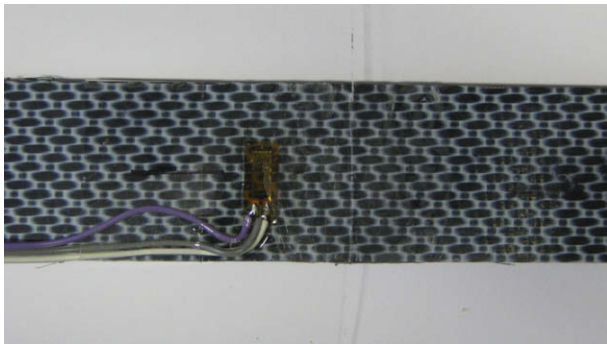


Fig. 24. Externally bonded optical fibre sensor on carbon/PPS laminate.

Finally, the transverse strain measurement was repeated with an external optical fibre sensor. This time, a special mould was designed to create a very thin bonding line. The results are shown in Fig. 24.

The optical fibre sensor was read out with an FBG-scan interrogator. Due to the limited sample rate of the interrogator, the cyclic test was paused after every unloading step and then both the transverse strain gauge and external optical fibre sensor were read out in unloaded condition. First, three loading cycles till 100 MPa were performed and then the maximum stress was gradually increased with 50 MPa for each cycle. Fig. 25 shows the transverse strain measurement for the quasi-static cyclic test on the $[(0^\circ,90^\circ)]_{4s}$ carbon/PPS specimen N9, from the 250 MPa loading cycle till the 550 MPa loading cycle. Considering the fact that the measured strains are very low, there is a good agreement between the strain gauge and the optical fibre in the unloaded condition.

This research fits into a larger investigation into the fatigue behaviour of this material. In all fatigue tests that are conducted

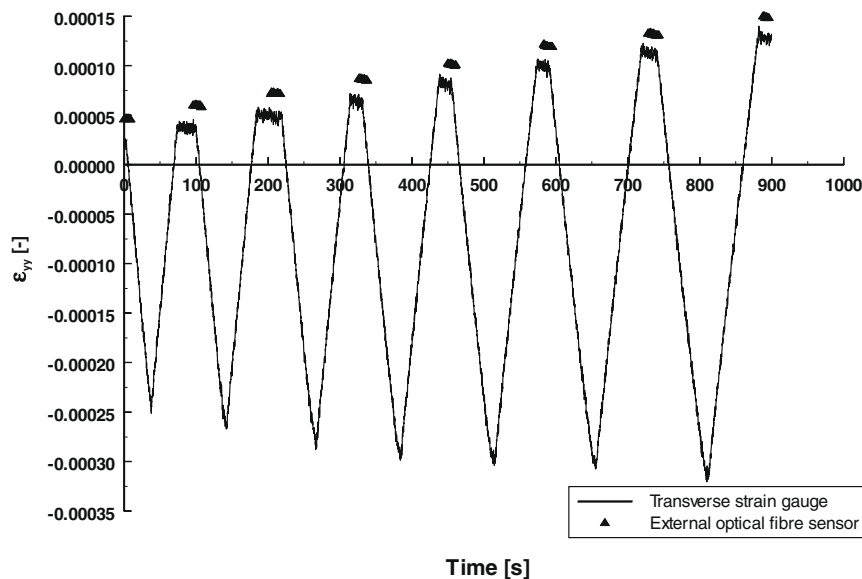


Fig. 25. Transverse strain measurement by transverse strain gauge and external optical fibre sensor for quasi-static cyclic test on $[(0^\circ/90^\circ)]_{4s}$ carbon/PPS specimen N9.

now in the laboratory, the evolution of the Poisson's ratio is measured by default. In a set of about 20 fatigue tests, we always observe the same behaviour, with very little scatter on the peculiar shape of the $v_{xy}-\varepsilon_{xx}$ curve.

6. Conclusions

It has been demonstrated that both the amplitude and the shape of the $v_{xy}-\varepsilon_{xx}$ curve change when damage is present in a composite laminate. The static evolution of the Poisson's ratio is the envelope that encloses the cyclic $v_{xy}-\varepsilon_{xx}$ curves in a broad range.

Further research has indicated that the transverse strain measurement can be considered reliable and that the observed behaviour is not due to improper strain transfer in the bonding layer of the strain gauge. Finally, it has been shown that the value of the Poisson's ratio can also be used as a damage indicator for other material combinations than glass/epoxy.

More research is necessary on the statistical interpretation of the observed behaviour of the Poisson's ratio.

Acknowledgements

The author W. Van Paepegem gratefully acknowledges his finance through a grant of the Fund for Scientific Research – Flanders (FWO). The authors also express their gratitude to Syncoglas for their support and technical collaboration.

References

- [1] Mallick PK. Composites engineering handbook. New York: Marcel Dekker Inc.; 1997.
- [2] Herakovich CT. Mechanics of fibrous composites. New York: John Wiley & Sons, Inc.; 1998.
- [3] Schulte K, Baron Ch, Neubert H, Bader MG, Boniface L, Wevers M, et al. Damage development in carbon fibre epoxy laminates: cyclic loading. In: Proceedings of the MRS-symposium advanced materials for transport, Strassbourg; November 1985. 8p.
- [4] Schulte K, Reese E, Chou TW. Fatigue behaviour and damage development in woven fabric and hybrid fabric composites. In: Matthews FL, Buskell NCR, Hodgkinson JM, Morton J, editors. Sixth international conference on composite materials (ICCM-VI) and second European conference on composite materials (ECCM-II). Proceedings, 20–24 July 1987, vol. 4. London (UK): Elsevier; 1987. p. 489–99.
- [5] Schulte K. Stiffness reduction and development of longitudinal cracks during fatigue loading of composite laminates. In: Cardon AH, Verchery G, editors. Mechanical characterisation of load bearing fibre composite laminates. Proceedings of the European mechanics colloquium, 29–31 August 1984, vol. 182. Brussels (Belgium): Elsevier; 1984. p. 36–54.
- [6] Fujii T, Amijima S, Okubo K. Microscopic fatigue processes in a plain-weave glass-fibre composite. Compos Sci Technol 1993;49:327–33.
- [7] Pandita SD, Huysmans G, Wevers M, Verpoest I. Tensile fatigue behaviour of glass-plain weave fabric composites in the on and off-axis directions. In: Proceedings of the fifth international conference on textile composites, Leuven, Belgium; 18–20 September 2000.
- [8] Sidoroff F, Subagio B. Fatigue damage modeling of composite materials from bending tests. In: Matthews FL, Buskell NCR, Hodgkinson JM, Morton J, editors. Sixth international conference on composite materials (ICCM-VI) and second European conference on composite materials (ECCM-II). Proceedings, 20–24 July 1987, vol. 4. London (UK): Elsevier; 1987. p. 432–9.
- [9] Vieilleveigne S, Jeulin D, Renard J, Sicot N. Modelling of the fatigue behaviour of a unidirectional glass epoxy composite submitted to fatigue loadings. In: Degallaix S, Bathias C, Fougères R, editors. International conference on fatigue of composites. Proceedings, 3–5 June 1997. Paris (France): La Société Française de Métallurgie et de Matériaux; 1997. p. 424–30.
- [10] Kawai M. Damage mechanics model for off-axis fatigue behaviour of unidirectional carbon fibre-reinforced composites at room and high temperatures. In: Massard T, Vautrin A, editors. Proceedings of the twelfth international conference on composite materials (ICCM-12), Paris, France; 5–9 July 1999. 322p.
- [11] Hwang W, Han KS. Fatigue of composites – fatigue modulus concept and life prediction. J Compos Mater 1986;20:154–65.
- [12] Hwang W, Han KS. Cumulative damage models and multi-stress fatigue life prediction. J Compos Mater 1986;20:125–53.
- [13] Whitworth HA. Modelling stiffness reduction of graphite epoxy composite laminates. J Compos Mater 1987;21:362–72.
- [14] Yang JN, Jones DL, Yang SH, Meskini A. A stiffness degradation model for graphite/epoxy laminates. J Compos Mater 1990;24:753–69.
- [15] Brøndsted P, Andersen SI, Lilholt H. Fatigue damage accumulation and lifetime prediction of GFRP materials under block loading and stochastic loading. In: Andersen SI, Brøndsted P, Lilholt H, Lystrup Aa, Rheinländer JT, Sørensen BF, et al., editors. Polymeric composites – expanding the limits. Proceedings of the 18th Risø international symposium on materials science, 1–5 September 1997. Roskilde (Denmark): Risø International Laboratory; 1997. p. 269–78.
- [16] Brøndsted P, Lilholt H, Andersen SI. Fatigue damage prediction by measurements of the stiffness degradation in polymer matrix composites. In: Degallaix S, Bathias C, Fougères R, editors. International conference on fatigue of composites. Proceedings, 3–5 June 1997. Paris (France): La Société Française de Métallurgie et de Matériaux; 1997. p. 370–7.
- [17] Takemori MT. Dynamic Poisson's ratio: a novel technique to study interfacial adhesion. Polym Eng Sci 1978;18(16):1193–9.
- [18] Altstädt V. Hysteresismessungen zur charakterisierung der mechanisch-dynamischen eigenschaften von R-SMC. PhD thesis. Universität – Gesamthochschule Kassel; 1987 [in German].
- [19] Bandoh S, Matsumura K, Zako M, Shiino T, Kurashiki T. On the detection of fatigue damage in CFRP by measuring Poisson's ratio. In: Hui D, editor. Eighth international conference on composites engineering (ICCE/8). Proceedings, Tenerife, Spain; 5–11 August 2001. p. 55–6.
- [20] Pidaparti RM, Vogt A. Experimental investigation of Poisson's ratio as a damage parameter for bone fatigue. J Biomed Mater Res Part A 2002;59(2):282–7.
- [21] Talreja R. Stiffness properties of composite laminates with matrix cracking and interior delamination. Eng Fract Mech 1986;25(5/6):751–62.
- [22] Hashin Z. Analysis of stiffness reduction of cracked cross-ply laminates. Eng Fract Mech 1986;25(5/6):771–8.
- [23] El Mahi A, Berthelot J-M, Brillaud J. Stiffness reduction and energy release rate of cross-ply laminates during fatigue tests. Compos Struct 1995;30:123–30.
- [24] Joffe R, Varna J. Analytical modeling of stiffness reduction in symmetric and balanced laminates due to cracks in 90° layers. Compos Sci Technol 1999;59:1641–52.
- [25] Pradhan B, Venu Kumar N, Rao NS. Stiffness degradation resulting from 90° ply cracking in angle-ply composite laminates. Compos Sci Technol 1999;59:1543–52.
- [26] Talreja R, Yalvac S, Yats LD, Wetters DG. Transverse cracking and stiffness reduction in cross-ply laminates of different matrix toughness. J Compos Mater 1992;26(11):1644–63.
- [27] Sol H, de Wilde WP. Identification of elastic properties of composite materials using resonant frequencies. In: Brebbia CA, de Wilde WP, Blain WR, editors. Proceedings of the international conference computer aided design in composite material technology. Southampton: Springer-Verlag; 1988. p. 273–80.
- [28] Sol H. Identification of the complex moduli of composite materials by a mixed numerical/experimental method. In: de Wilde WP, Blain WR, editors. Proceedings of the second international conference on computer aided design in composite material technology, 25–27 April 1990. Brussels: Springer-Verlag; 1990. p. 267–79.
- [29] Van Paepegem W, De Baere I, Degrieck J. Modelling the nonlinear shear stress-strain response of glass fibre-reinforced composites. Part I: experimental results. Compos Sci Technol 2005;66(10):1455–64.
- [30] Van Paepegem W, De Baere I, Degrieck J. Modelling the nonlinear shear stress-strain response of glass fibre-reinforced composites. Part II: model development and finite element simulations. Compos Sci Technol 2005;66(10):1465–78.
- [31] De Baere I, Van Paepegem W, Degrieck J, Sol H, Van Hemelrijck D, Petreli A. Comparison of different identification techniques for measurement of quasi-zero Poisson's ratio of fabric reinforced laminates. Composites Part A 2007;38(9):2047–54.